axioms

MDPI

Article

Inspection of a Time-Delayed Excited Damping Duffing Oscillator

Khalid Alluhydan [1], Galal M. Moatimid [2], T. S. Amer [3] and A. A. Galal [4,*]

[1] Department of Mechanical Engineering, College of Engineering, King Saud University, P.O. Box 800, Riyadh 11421, Saudi Arabia; kalluhydan@ksu.edu.sa
[2] Department of Mathematics, Faculty of Education, Ain Shams University, Cairo 11566, Egypt; gal_moa@edu.asu.edu.eg
[3] Department of Mathematics, Faculty of Science, Tanta University, Tanta 31527, Egypt; tarek.saleh@science.tanta.edu.eg
[4] Department of Engineering Physics and Mathematics, Faculty of Engineering, Tanta University, Tanta 31734, Egypt
* Correspondence: abdallah.galal@f-eng.tanta.edu.eg

Abstract: This paper examines a time delay in position and velocity to minimize the nonlinear vibration of an excited Duffing oscillator (DO). This model is highly beneficial for capturing the nonlinear characteristics of many different applications in engineering. To achieve an estimated uniform solution to the problem under consideration, a modified homotopy perturbation method (HPM) is utilized. This adaptation produces a more accurate precise approximation with a numerical solution (NS). This is obtained by employing Mathematica software 12 (MS) in comparison with the analytical solution (AS). The comparison signifies a good match between the two methodologies. The comparison is made with the aid of the NS. Consequently, the work allows for a qualitative assessment of the results of a representative analytical approximation approach. A promising stability analysis for the unforced system is performed. The time history of the accomplished results is illustrated in light of a diverse range of physical frequency and time-delay aspects. The outcomes are theoretically discussed and numerically explained with a set of graphs. The nonlinear structured prototype is examined via the multiple-scale procedure. It investigates how various controlling limits affect the organization of vibration performances. As a key assumption, according to cubic nonlinearity, two significant examples of resonance, sub-harmonic and super-harmonic, are explored. The obtained modulation equations, in these situations, are quantitatively investigated with regard to the influence of the applied backgrounds.

Keywords: Duffing oscillator; modified homotopy perturbation method; nonlinear vibrations; time delay; external excitation

MSC: 65P40; 70k20; 70Q05; 74H45

check for updates

Citation: Alluhydan, K.; Moatimid, G.M.; Amer, T.S.; Galal, A.A. Inspection of a Time-Delayed Excited Damping Duffing Oscillator. *Axioms* **2024**, *13*, 416. https://doi.org/10.3390/axioms13060416

Academic Editor: Simeon Reich

Received: 6 May 2024
Revised: 2 June 2024
Accepted: 12 June 2024
Published: 20 June 2024

Copyright: © 2024 by the authors. Licensee MDPI, Basel, Switzerland. This article is an open access article distributed under the terms and conditions of the Creative Commons Attribution (CC BY) license (https://creativecommons.org/licenses/by/4.0/).

1. Introduction

Nonlinear oscillation systems present a challenging mathematical problem, garnering recent interest from mathematicians, researchers, engineers, and scientists. Exploring the solutions to these equations is crucial for professionals in mathematics, physics, and engineering. The past few decades have seen increased attention given to understanding nonlinear oscillators, particularly in dynamical systems where nonlinear differential equations with unknown solutions are prevalent. Predicting dynamic response behavior and establishing frequency–amplitude connections necessitate employing approximate numerical or analytical approaches. The DO is a nonlinear ordinary differential equation (ODE) that is employed to represent specific oscillations that are both damped and driven. This is an instance of a dynamical system that demonstrates chaotic behavior. In addition, the DO has demonstrated the occurrence of jump resonance phenomena in its frequency response, which can be described as a form of frequency hysteresis behavior. The DO is a basic forced

oscillator that is used in a variety of fields, including physics, engineering, electronics, and many others. The dynamics of oscillators are playing a growing, significant part in the study of current nonlinear science. Investigations into Melnikov chaos and the impact of nonlinear dissipation on DO basin borders have been conducted [1,2]. Investigations have been made into DO chaotic behavior when subjected to harmonic external inspirations. The required conditions for the system of chaotic motion were found by applying the Melnikov approach. Their findings demonstrated that when damping went over the threshold of Melnikov chaos, the geometry of the basin borders of attraction took on fractal characteristics. Among the most well-known examples of self-excited systems is the Rayleigh oscillator. A dynamic collaboration concerning a cantilever beam with nonlinear dampening and rigidity performance, described by the DO, and a non-ideal motor connected to the end of a shaft was analytically and numerically studied [3]. By using the combination compartment coordinate structure technique, the comprehensive bifurcations in the DO, such as emergency and basin boundary conversion, were investigated [4]. The latter study separated the continuous state space into the cell state space with various measurements and proposed a novel vision of a combined cell coordinate structure. Attractors, basins of attractors, basin borders, saddles, and invariant manifolds may all be easily found for a dynamical system, and any area of a state space can be streamlined using this technique [5]. The outcomes of their theoretical work were shown in numerical phase plots. An algebraic approach was used to investigate the three challenges of the nonlinear ODE in the realm of vibration, known as the Van der Pol, Rayleigh, and DOs challenges [6]. It was possible to conclude from comparisons of the obtained results, using the algebraic technique and the NS, that the algebraic method may be used to analyze a selection of differential equations, especially challenging ones. The initial integrals of the DO were given a thorough algebraic characterization [7]. In light of the great importance of the DO in an extensive domain of applications in numerous areas, the existing problem is concerning. The methodology of the current paper aims to treat nonlinearity in an excited DO, incorporating a delayed representation of position and velocity. This additional representation serves as a technique to further dampen nonlinear oscillations.

The research focus on controlling nonlinear oscillations through time-delayed feedback has strengthened in recent decades. Recognizing time delays as a primary source of reduced process performance and system instability, particularly in engineering practices, highlights the ongoing necessity of investigating system stability with time delays. Stability analysis, conducted with minor perturbations near the critical point, has been performed for nonlinear time-delayed structures [8]. Time-delayed ODEs have been useful in describing the dynamics of various control systems, considering delays that arise from factors like feedback-loop-related actuators, sensors, and field networks. Additionally, various distinct procedures concerning the dynamics of waves have been modeled using time-delay systems [9,10]. Fuzzy time-delay system stage settings were represented as complex numbers, and a numerical methodology was utilized to find the solution. Models concerning the interchange of nonnegative quantities between subsystems or compartments were developed [11]. These models are fundamental in comprehending these processes and are widely used in the biological and physical disciplines. Dissipative theory was employed in a specific way to find the Lyapunov–Krasovskii function [12]. Delay-dependent and delay-independent analyses were used to categorize the stability study of time-delay practices. A method to recognize nonlinear dynamical structures was suggested [13,14]. Nonlinear structures with time delays were added to the light optimization methodology. The suggested approach combines machine learning cross-validation techniques for an automated scheme to remove dependency on initial conditions (ICs) and filter out the noise. The concept of time delay served as additional protection against the nonlinear vibrations of the inspected structure. To decrease the nonlinear vibrations of the considered system, a time-delayed position velocity control is proposed. However, the time delay may disintegrate the implementation of switching systems or worse lead to system instability. Subsequently, this paper examines the DO in the presence of a time delay. While

much research has been conducted on time-delayed systems, this study specifically emphasizes their critical significance. Additionally, the modified homotopy perturbation method (HPM) is employed to enhance the precision of the projected solution, providing a more accurate estimation. The main objective of this work is to demonstrate the accuracy of an analytical technique by comparing it with numerical solutions. This comparison allows for a qualitative evaluation of the results

Historically, ODEs and partial differential equations (PDEs) have proven effective in solving diverse scientific problems such as mathematical modeling, hydrodynamics, and theoretical physics. However, accurate solutions are limited for certain concerns. To address this, the NS or a combination with analytical perturbation methods is often employed. Traditional perturbation approaches were typically relying on minor factors, but analytical solutions were preferred. The challenge lies in small parameter requirements in traditional perturbation theory, which represent a significant obstacle for researchers. Chinese mathematician Prof. He introduced the HPM [15,16], notable for its simplicity as it did not necessitate the presence of a small parameter. This method has evolved into a robust and promising strategy applicable to various classes of ODEs. The HPM will be explored further, dividing the problem into two parts using the embedded homotopy parameter as a constraining element. The HPM is utilized [17] to solve various problems with an exact solution or an accurate approximation. It is demonstrated how this approach's convergence has been slightly improved. To obtain perfect explanations for both linear and nonlinear ODEs, an update of the HPM is provided. The main idea of the procedure relies on consistently guessing an acceptable function, such as a power series. Through the elimination of the initial order, all subsequent orders are determined. Under constrained conditions, the basic equation is changed to a challenging nonlinear ODE. The methodology of MS is used to confirm the possibility of the solution. Once more, in light of the significance of the ODE in a variety of situations in real-world manufacturing, under particular circumstances, the magnetic spherical pendulum's governing equation of motion can produce a DO [18,19]. The goal is to solve this problem analytically using a bounding technique. In reality, the HPM and its development became a method for dealing with various classes of nonlinear dynamics. This method performs the calculations quicker than previous methods, overcomes computational complexities, and uses less computer memory. It is straightforward, strong, efficient, and promising. Because using the HPM provides a lot of benefits, it is employed in analyzing the current problem. The current paper uses the HPM, which has been successfully applied to a wide variety of problems in physics, engineering, and applied mathematics. It provides a powerful and flexible tool for tackling nonlinear ODEs, especially when exact analytical solutions are difficult or impossible to obtain. Additionally, the current paper makes some modifications to this technique. Therefore, this approach overcomes calculation complexity, requires less computer memory, and has a faster calculation time than the previous methods. Accordingly, it is simple, powerful, effective, and promising.

The study of time-delayed controllers to stimulate the DO has possible advantages in engineering, physics, communication theory, and biology, in agreement with the relevance of the aforementioned components. It has been covered in a wide range of articles on many topics. The preceding problem with position and velocity delays is examined in this paper as follows:

$$\ddot{\theta}(t) + \omega^2\theta(t) + 2\mu\dot{\theta}(t) + \alpha\dot{\theta}^3(t) + \beta\theta^3(t) = f\cos\Omega t + \gamma\theta(t-\tau) + \zeta\dot{\theta}(t-\tau), \quad (1)$$

where a record of all the symbols in Equation (1) is provided before the introduction section.

It should be noticed, for the sake of straightforwardness, that the governing equation of motion (1) has been formulated in a non-dimensional form.

2. Methodology of the Improved HPM

The HPM can provide a diverse range of estimated solutions, as is clearly identified in our previous paper [19]. One of these methodologies provides a classical solution with

secular evidence which is physically unsatisfactory. A complementary approach uses the expanded frequency to produce an acceptable solution; the generated solutions do not satisfy the numerical one. Accordingly, the HPM necessity subsequently is changed once again. To investigate the effects of the delay factor, which is better for avoiding bifurcations and reducing vibration, we may thus re-scrutinize the elementary homotopy equation by applying an innovative $\theta(t,\rho)$ expansion in place of the straight expansion. Grounded on our existing works, we assume that the approach can be enhanced as previously indicated [19]. The subsequent are the processes to achieve the desired solution:

The essential homotopy equation provides the base for the HPM concept [18,19]. Additionally, in this case, the homotopy equation may be constructed as given by He [15] by the formula:

$$\ddot{\theta} + \omega^2\theta + \rho[2\mu\dot{\theta} + \alpha\,\dot{\theta}^3 + \beta\,\theta^3 - f\cos\Omega t - \gamma\,\theta(t-\tau) - \zeta\,\dot{\theta}(t-\tau)] = 0, \qquad \rho \in [0,1] \quad (2)$$

As is well known, the standard HPM produces secular terms; unfortunately, we do not have the authority to cancel these terms. The cancelation of these terms yields the zero solution which is known as the trivial solution. Therefore, the adaptation of the HPM is urgent. The coming exponential factor was previously provided [20].

$$\theta(t,\rho) = e^{-\rho\tau\,t}\Big\{\theta_0(t) + \rho\,\theta_1(t) + \rho^2\theta_2(t) + \ldots\Big\}. \quad (3)$$

Relating to the procedure of the beforehand realized inspection, the recognized expected frequency can be augmented as exposed beneath [19]. Furthermore, the parameter addresses the natural frequency of the problem ω. The forthcoming stability inquiry will rely on the enlarged artificial frequency analysis σ^2, as exemplified in Ref. [21]. Following this methodology, an increased frequency may be expressed as

$$\sigma^2 = \omega^2 + \sum_{i=1}^{n} \rho^i \omega_i, \quad (4)$$

where σ signifies a new nonlinear frequency.

It is reasonable to provide the ICs for the analysis of Equation (1) as:

$$\theta(0) = 0, \qquad \dot{\theta}(0) = 1. \quad (5)$$

One must add modification as given in Equation (3) to the homotopy equation in order to produce the required solution. As a consequence, the exact analytical preparation of the zero-order equation is:

$$\theta_0(t) = \frac{1}{\sigma}\sin\sigma t. \quad (6)$$

Consequently, one realizes

$$\theta_0(t-\tau) = \frac{1}{\sigma}\sin\sigma(t-\tau), \quad (7)$$

and

$$\dot{\theta}_0(t-\tau) = \cos\sigma(t-\tau). \quad (8)$$

The first-order challenge of the homotopy Equation (2) could be generated by:

$$\ddot{\theta}_1 + \sigma^2\theta_1 = \omega_1\theta_0 - 2\mu\dot{\theta}_0 - \alpha\,\dot{\theta}_0^3 - \beta\,\theta_0^3 + f\cos\Omega t + \gamma\,\theta_0(t-\tau) + \zeta\,\dot{\theta}_0(t-\tau) + 2\tau\ \dot{\theta}_0. \quad (9)$$

Equation (6) to (8), along with Equation (9), collectively support

$$\begin{array}{l}\ddot{\theta}_1+\sigma^2\theta_1=\frac{1}{4\sigma^3}\left(4f\sigma^3\cos(t\Omega)-\alpha\sigma^3\cos(3\sigma t)+\beta\sin(3\sigma t)\right)\\+\frac{\cos(\sigma t)}{4\sigma^3}\left(-3\alpha\sigma^3-4\gamma\sigma^2\sin(\sigma\tau)+4\zeta\sigma^3\cos(\sigma\tau)-8\mu\sigma^3+8\sigma^3\tau\right)\\+\frac{\sin(\sigma t)}{4\sigma^3}\left(-3\beta+4\gamma\sigma^2\cos(\sigma\tau)+4\zeta\sigma^3\sin(\sigma\tau)+4\sigma^2(\sigma^2-\omega^2)\right).\end{array}\tag{10}$$

Traditionally, the secular functions must be eliminated to obtain a uniformly valid statement. For this objective, the measurements of the trigonometric functions $\cos\sigma\tau$ and $\sin\sigma\tau$ should be disregarded. Therefore, one finds

$$-3\alpha\sigma^3-4\gamma\sigma^2\sin(\sigma\tau)+4\zeta\sigma^3\cos(\sigma\tau)-8\mu\sigma^3+8\sigma^3\tau=0,\tag{11}$$

and

$$-3\beta+4\gamma\sigma^2\cos(\sigma\tau)+4\zeta\sigma^3\sin(\sigma\tau)+4\sigma^2(\sigma^2-\omega^2)=0.\tag{12}$$

Solving Equations (11) and (12), one obtains

$$\cos\sigma\tau=-\frac{-3\alpha\zeta\sigma^4-3\beta\gamma+4\gamma\sigma^2\left(\sigma^2-\omega^2\right)-8\zeta\mu\sigma^4+8\zeta\sigma^4\tau}{4\sigma^2(\gamma^2+\zeta^2\sigma^2)},\tag{13}$$

and

$$\sin\sigma\tau=-\frac{-3\beta\zeta+3\alpha\gamma\sigma^2+8\gamma\mu\sigma^2-8\gamma\sigma^2\tau+4\zeta\sigma^2\left(\sigma^2-\omega^2\right)}{4\sigma(\gamma^2+\zeta^2\sigma^2)}.\tag{14}$$

Equations (4), (13) and (14) are taken together up to this point to generate the algebraic equations of the nonlinear frequency:

$$\begin{array}{l}-16\sigma^8+\sigma^6\left(-9\alpha^2+16\zeta^2-64\mu^2-48\alpha(\mu-\tau)+128\mu\tau-64\tau^2+32\omega^2\right)\\+\sigma^4\left(24\beta+16\gamma^2-16\omega^4\right)-24\beta\omega^2\sigma^2-9\beta^2=0.\end{array}\tag{15}$$

With regard to the first-order solution, the following ICs are considered:

$$\theta_1(0)=0,\qquad\dot{\theta}_1(0)=0.\tag{16}$$

The fundamental step in the process-constrained solution is defined by

$$\begin{array}{c}\theta_1(t)=\frac{3\beta\sigma^2\sin(\sigma t)-\beta\sigma^2\sin(3\sigma t)-3\beta\Omega^2\sin(\sigma t)+\beta\Omega^2\sin(3\sigma t)}{32\sigma^5(\sigma^2-\Omega^2)}\\+\frac{\alpha\cos(3\sigma t)+\alpha\cos(\sigma t)}{32\sigma^2}+\frac{f\cos(t\Omega)-f\cos(\sigma t)}{(\sigma^2-\Omega^2)}.\end{array}\tag{17}$$

As a consequence, up to the first order, the approximated uniform solution of the basic equation of motion described in Equation (1) might be expressed as:

$$\begin{array}{l}\theta(t)=\lim\limits_{\rho\to1}e^{-\rho t\tau}(\theta_0(t)+\rho\theta_1(t))=\\\left(\begin{array}{c}\frac{1}{\sigma}\sin\sigma t+\frac{3\beta\sigma^2\sin(\sigma t)-\beta\sigma^2\sin(3\sigma t)-3\beta\Omega^2\sin(\sigma t)+\beta\Omega^2\sin(3\sigma t)}{32\sigma^5(\sigma^2-\Omega^2)}\\+\frac{\alpha\cos(3\sigma t)+\alpha\cos(\sigma t)}{32\sigma^2}+\frac{f\cos(\Omega t)-f\cos(\sigma t)}{(\sigma^2-\Omega^2)}\end{array}\right)e^{-t\tau},\end{array}\tag{18}$$

where the functions $\theta_0(t)$ and $\theta_1(t)$ are found through Equations (6) and (17), correspondingly.

For greater convenience, after the analytical process of obtaining the approximate solution to the fundamental equation of motion, a numerical methodology becomes essential. As demonstrated, coupling the homotopy perturbation method (HPM) with the nonlinear frequency concept results in what is termed the analytical solution (AS). MS is used to graph both the numerical solution of the original ODE and the numerical solution (NS) of

the approximate solution provided in Equation (18). This procedure is carried out using a sample-chosen system as follows:

$$\mu = 0.05, \quad \omega = 4.5, \quad \alpha = 2.5, \quad \beta = -2, \quad \gamma = 1.05, \quad \zeta = 1, \quad \tau = 0.6, \quad f = 0.5, \quad \Omega = 25.$$

Ordinarily, the nonlinear frequency values are determined independently of the external excitation force and its frequency. Fortunately, the MS, changing the prior data in the characteristic Equation (15) results in eight alternative real roots. The computations that followed considered the value $\sigma = 4.16303$. For increasing convenience, the analytical estimated solution may be numerically plotted, which is referred to as NS, by means of MS. Therefore, Figure 1 shows the comparison between these solutions, which reveals a good agreement between them, especially in the second half of the investigated time interval. The noted decaying forms of the drawn curves increase with time, which reveals that the behaviors of both solutions have steady forms.

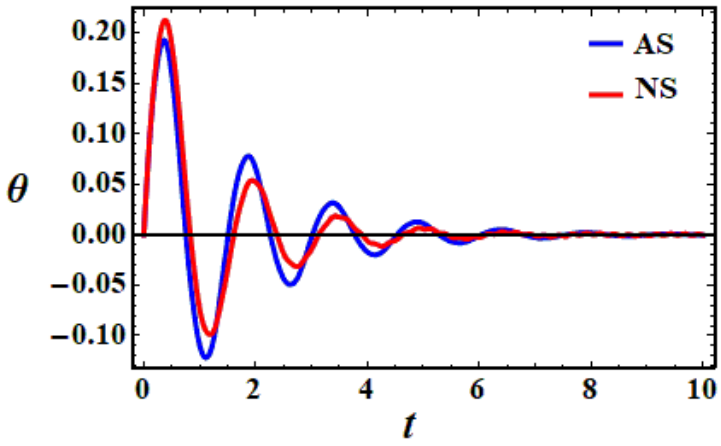

Figure 1. Comparison between AS and NS solutions.

It should be noted that the modified HPM introduces the exponential $Exp(-\rho\tau t)$ to indicate the decaying in the perturbed solution. In the absence of this term of the perturbed expansion, with the aid of the concept of expanded frequency [18], it produces an oscillatory solution. Actually, in this case, the decaying numerical solution becomes very different from the approximate solution.

3. Outcomes for Resonance Case

In practice, excitation frequency happens in collections. A resonance occurs when the system frequency and the frequencies of external loads are significantly met. In this case, the resulting vibrations make a large amplitude. This may be used in applications in both positive and negative ways. One of the resonance positive effects is the resonance technology, which is utilized to prevent a system from oscillating when it is excited. In addition to the impacts of resonance, excitations lead to the damage of airplanes and buildings.

3.1. Primary Resonance ($\Omega \cong \omega$)

In the initial resonance stage, the machinery would respond significantly to high-excitation energies with little motivation. Consequently, the following is how the circumstance of the homotopy equation might be written:

$$H(\theta, \rho) = L(\theta) + \rho N(\theta), \qquad \rho \in [0, 1], \tag{19}$$

where $L(\theta)$ and $N(\theta)$ are the linear and nonlinear portions of the specified equation, correspondingly. ρ is identified as the implanted synthetic homotopy factor.

As considered in the homotopy equation in (2), one can write:

$$L(y) = \ddot{\theta} + \omega^2\theta, \tag{20}$$

$$N(y) = 2\mu\dot{\theta} + \alpha\dot{\theta}^3 + \beta\theta^3 - f\cos\Omega t - \gamma\,\theta(t-\tau) - \zeta\,\dot{\theta}(t-\tau). \tag{21}$$

Accordingly, Equation (1) may be written as:

$$H(\theta,\rho) = \ddot{\theta} + \omega^2\theta + \rho[2\mu\dot{\theta} + \alpha\,\dot{\theta}^3 + \beta\,\theta^3 - f\cos\Omega t - \gamma\,\theta(t-\tau) - \zeta\,\dot{\theta}(t-\tau)]. \tag{22}$$

It is possible to display a two-time-scale enlargement without suffering any applicability loss. Therefore, one can write:

$$\theta(t,\rho) = \theta_0(T_0,T_1) + \rho\theta_1(T_0,T_1) + O(\rho^2), \tag{23}$$

$$\theta(t-\tau,\rho) = \theta_0(T_0-\tau,T_1-\rho\tau) + \rho\theta_1(T_0-\tau,T_1-\rho\tau) + O(\rho^2), \tag{24}$$

where $T_0 = t$ and $T_1 = \rho t$. It follows that the time derivatives $\frac{d}{dt}$ and $\frac{d^2}{dt^2}$ may be formulated through the time scales T_0 and T_1 as [22,23]:

$$\frac{d}{dt} = D_0 + \rho D_1, \quad \frac{d^2}{dt^2} = D_0^2 + 2\rho D_0 D_1,; \qquad D_j = \frac{\partial}{\partial T_j}, \qquad (j = 0,1). \tag{25}$$

Substituting Equations (23)–(25) into Equation (22), then equating coefficients of the associated exponents of ρ, we obtain

$$\rho^0: \quad D_0^2\theta_0 + \omega^2\theta_0 = 0, \tag{26}$$

$$\begin{aligned}\rho^1: \quad D_0^2\theta_1 + \omega^2\theta_1 = {} & -2D_0D_1\theta_0 - 2\mu D_0\theta_0 - \beta\theta_0^3 + \gamma\theta_0(T_0-\tau,T_1-\rho\tau) \\ & -\alpha(D_0\theta_0\ )^3 + \zeta D_0\theta_0(T_0-\tau,T_1-\rho\tau) \ + F\cos(\Omega T_0).\end{aligned} \tag{27}$$

Equation (26) can be expressed as:

$$\theta_0(T_0,T_1) = A(T_1)e^{i\omega T_0} + c.c., \tag{28}$$

where *c.c.* indicates the complex conjugate of the previous terms.

Substituting Equation (28) on Equation (27), one achieves

$$\begin{aligned}D_0^2\theta_1 + \omega^2\theta_1 = {} & e^{i\omega T_0}(-2i\omega D_1A - 3i\alpha\omega^3A^2\overline{A} - 2i\mu\omega A - 3\beta A^2\overline{A} + e^{-i\tau\omega}\gamma A \\ & + ie^{-i\tau\omega}\zeta\omega A + \tfrac{1}{2}e^{i\sigma T_1}f) + A^3e^{3i\omega T_0}(i\alpha\omega^3 - \beta) + c.c.\end{aligned} \tag{29}$$

The secular elements should be eliminated in order to achieve a consistent advantageous development. The function $e^{\pm i\omega T_0}$ coefficients must be removed in order to balance out such terms. Consequently, we arrive at the appropriate solvability situation:

$$-2i\omega D_1A + A[-2i\mu\omega + e^{-i\tau\omega}(\gamma + i\zeta\omega)] - 3A^2\overline{A}(i\alpha\omega^3 + \beta) + \frac{f}{2}e^{i\sigma T_1} = 0. \tag{30}$$

Considerably, the outcome of Equation (29) may be expressed as:

$$\theta_1(T_0,T_1) = -\frac{1}{8\omega^2}A^3e^{3i\omega T_0}(i\alpha\omega^3 - \beta) + c.c. \tag{31}$$

Equation (30) can be written once again as

$$-2i\omega\frac{dA}{dt} + A\,[-2i\mu\omega + e^{-i\tau\omega}(\gamma + i\zeta\omega)] - 3A^2\overline{A}(i\alpha\omega^3 + \beta) + \frac{f}{2}e^{i\sigma t} = 0. \tag{32}$$

Succeeding the construction of $A(t)$ may be formulated like [24]

$$A(t) = \frac{1}{2}a(t)e^{i\psi(t)}, \tag{33}$$

where $a(t)$ and $\psi(t)$ are two actual time-related functions. They stand for the system's intensity and adjusted phase-angle vibrations, correspondingly. After splitting the real and imaginary components of Equation (33) and inserting them into Equation (32), one achieves the corresponding amplitude-phase adjustments:

$$\dot{a} = \frac{1}{\omega}(4a\zeta\omega\cos\omega\tau - 4a\gamma\sin\omega\tau + 4f\sin\varphi - 8a\mu\omega - 3a^3\alpha\omega^3), \tag{34}$$

$$\dot{\phi} = \frac{1}{8a\omega}(8a\sigma\omega - 3a^3\beta + 4f\cos\varphi + 4a\gamma\cos\omega\tau + 4a\zeta\omega\sin\omega\tau). \tag{35}$$

Herein, $\phi = \sigma t - \psi$.

To use the steady-state oscillations, one finds $\dot{a} = \dot{\phi} = 0$, and consequently, Equations (34) and (35) are developed

$$4f\cos\varphi = (3a^3\beta - 8a\sigma\omega - 4a\gamma\cos\omega\tau - 4a\zeta\omega\sin\omega\tau), \tag{36}$$

$$4f\sin\varphi = 8a\mu\omega + 3a^3\alpha\omega^3 - 4a\zeta\omega\cos\omega\tau + 4a\gamma\sin\omega\tau. \tag{37}$$

The combination of Equations (36) and (37) produces

$$\begin{aligned} 16f^2 = {} & (3a^3\beta - 8a\sigma\omega - 4a\gamma\cos\omega\tau - 4a\zeta\omega\sin\omega\tau)^2 \\ & + (8a\mu\omega + 3a^3\alpha\omega^3 - 4a\zeta\omega\cos\omega\tau + 4a\gamma\sin\omega\tau)^2. \end{aligned} \tag{38}$$

In the stability outline, the vibration amplitude will be designed against any restriction of the system similar a, f, γ, λ or τ. Such graphs would be demonstrated subsequently in the forthcoming part employing the MS. However, the linearized stability may be examined around the equilibrium points. Consequently, the subsequent steady-state solution may be assumed [20,25]:

$$a = a_{10} + a_{11}\,, \quad \phi = \phi_{10} + \phi_{11} \quad \Rightarrow \quad \dot{a} = \dot{a}_{11}, \quad \dot{\phi} = \dot{\phi}_{11}. \tag{39}$$

Equation (39) is substituted in Equations (34) and (35), and the linear terms of a_{11} and ϕ_{11} are only maintained. Subsequently, one finds

$$\begin{pmatrix} \dot{a}_{11} \\ \dot{\phi}_{11} \end{pmatrix} = \begin{pmatrix} -\frac{1}{\omega}(8\mu\omega + 9a_{10}^2\alpha\omega^3 - 4\zeta\omega\cos\omega\tau + 4\gamma\sin\omega\tau) & \frac{4f}{\omega}\cos\phi_{10} \\ -\frac{1}{4\omega}(3a\beta + \frac{2f}{a_{10}^2}\cos\phi_{10}) & -\frac{f}{2\omega a_{10}}\sin\phi_{10} \end{pmatrix} \begin{pmatrix} a_{11} \\ \phi_{11} \end{pmatrix}. \tag{40}$$

The Jacobian matrix eigenvalues can be used to study the solution stability of Equation (40). Therefore, one finds

$$\begin{vmatrix} s_1 - \lambda & s_2 \\ s_3 & s_4 - \lambda \end{vmatrix} = 0, \tag{41}$$

where

$$s_1 = \frac{1}{\omega}(-8\mu\omega - 9a_{10}^2\alpha\omega^3 + 4\zeta\omega\cos\omega\tau - 4\gamma\sin\omega\tau), \tag{42}$$

$$s_2 = -\frac{1}{\omega}(-3a_{10}^3\beta + 8a_{10}\sigma\omega + 4a_{10}\gamma\cos\omega\tau + 4a_{10}\zeta\omega\sin\omega\tau), \tag{43}$$

$$s_3 = \frac{1}{8\omega}[-9a_{10}\beta + \frac{1}{a_{10}}(8\sigma\omega + 4\gamma\cos\omega\tau + 4\zeta\omega\sin\omega\tau)], \tag{44}$$

$$s_4 = \frac{1}{8\omega}(-8\mu\omega - 3a^2\alpha\omega^3 + 4\zeta\omega\cos\omega\tau - 4\gamma\sin\omega\tau). \tag{45}$$

The characteristic equation then becomes

$$\lambda^2 - (s_1 + s_4)\lambda + s_1 s_4 - s_2 s_3 = 0. \tag{46}$$

Subsequently, the stability criteria might be formulated as:

$$s_1 + s_4 > 0\,, \quad s_1 s_4 - s_2 s_3 > 0. \tag{47}$$

The numerical interpretation of the previous theoretical outcomes will be illustrated in the next subsection.

3.2. Results and Discussions

The linear and nonlinear aspects of the location structure and velocity are regulated by employing controllers. The suggested prototype incorporates the closed-loop controller scheme of the time delay. The multiple scales method is used to develop two nonlinear algebraic equations that regulate the oscillation amplitude. These equations describe the phase angle of the control structure since the prototypical underneath study is a linear time-delayed dynamical scheme. Plotting of the stability diagrams for the loop delays is carried out using the algebraic equations that have been obtained. They investigated how control gains and loop delays affect the steady-state vibration amplitude. The collected outcomes show that the loop delays can have a significant impact on either increasing controller effectiveness or causing the controlled scheme to become unstable. The steady-state response of the scheme is thoroughly examined in this section for the various systems in the main resonance situation. Outcomes are described in the graphic styles as steady-state amplitudes against both the detuning parameter and the excitation force amplitude. The following figures are drawn by implementing the subsequent amounts of the system constraints: $\omega = 3.6$, $\mu = 0.05$, $\gamma = 0$, $\zeta = 0$, $\beta = 0$, $\tau = 0$, and $f = 0.5$ unless otherwise specified. Findings are displayed in graphic structures as steady-state amplitudes against both the detuning parameter σ and the external force f using frequency–response Equation (38).

3.2.1. Uncontrolled System

The main structure of the frequency–response curve (FRC) and the force–response curve prior to mechanism are established in Figure 2.

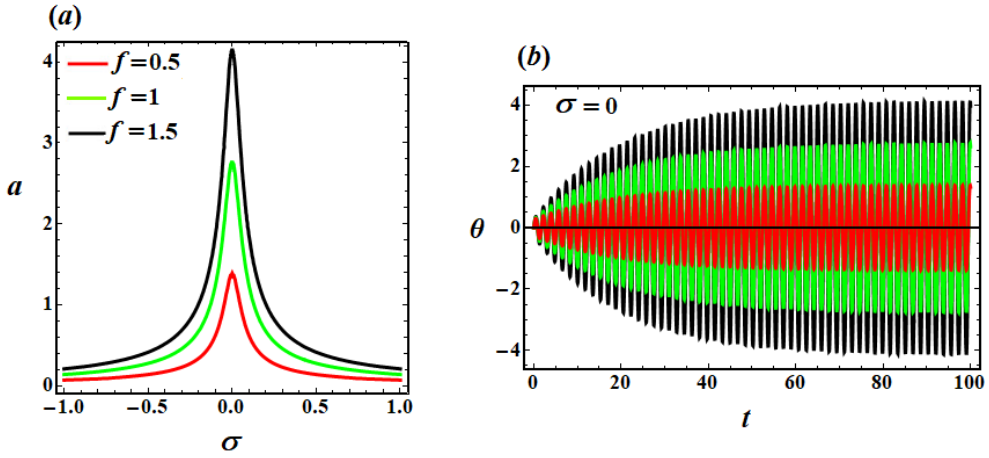

Figure 2. The FRC of the system before control $\omega = 3.6$, $\mu = 0.05$, $\gamma = 0$, $\zeta = 0$, $\beta = 0$, $\tau = 0$. (**a**) The structure FRC at three numerous quantities of the external force f, and (**b**) the temporal vibration of the structure corresponding to (**a**) while $\sigma = 0$ (i.e., $\Omega = \omega$) at the three distinct amounts of the external force $f = 0.5, 1$, and 1.5.

Figure 2a shows the force–response curves for numerous stages of the external amplitude f according to Equation (38). The amplitude of the response is contingent on the

detuning parameter σ and the amplitude of external f. It is clear that as the imposing amplitude rises, the nonlinearity will govern the system response. The curves of this figure signify the connection between the amplitude a and the parameter σ. The amplitudes of these curves increase with the rise in the amounts of f and they have symmetric forms about the vertical axis of symmetry $\sigma = 0$. Numerical simulation of at $\sigma = 0$ (i.e., when $\Omega = \omega$) at the mentioned amounts of the external force f and based on Equation (1) is illustrated in Figure 2b, to show the time history of θ . The plotted curves indicate that the time behavior of θ has a steady motion, where the amplitudes of the resulting oscillations increase till a specified value of time, and then they have steady manners.

3.2.2. Influence of Linear Position Control without Time-Delay

The implementation of the linear position controller in the absence of time delay of the nonlinear oscillation of the scheme is investigated as follows:

It is obvious in Figure 3a that the linear position controller affects the FRC either to the left-hand or the right-hand which are subject to the response gain γ. Consequently, it is possible to stop the high vibration amplitude of the structure by shifting its normal frequency far from the vibration frequency employing the linear position feedback controller. It is noted that each curve has an independent symmetric axis according to the values of γ, which accord with Equation (38). Calculation simulations for the controlled temporal vibrations corresponding to Figure 3a, $\sigma = -0.5$ (i.e., when $\Omega = \omega - 0.5$), are demonstrated in Figure 3b by analyzing the previous system of Equation (1). The inspection of the included curves shows that they have rapid oscillations at the beginning of the time interval. These oscillations vary between increasing and decreasing during the first quartile of the investigated time interval. Therefore, these oscillations become steady till the end of this interval, which means that the motion is free of chaos.

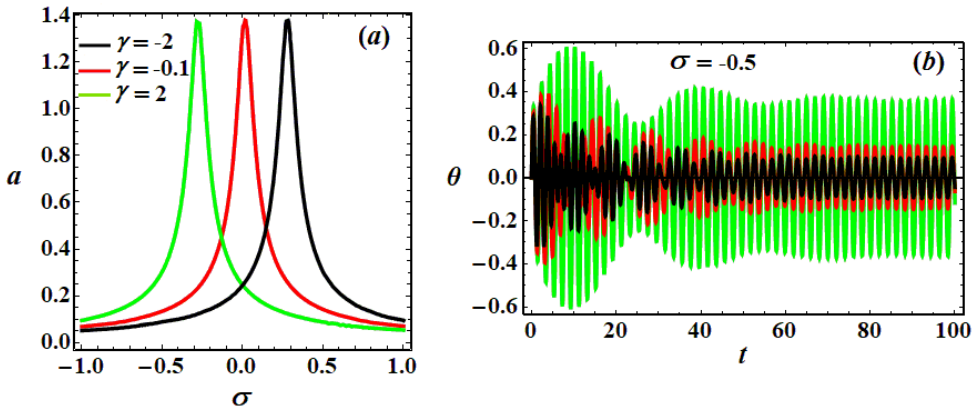

Figure 3. The impact of the linear position controller on the scheme FRC when the loop delay is zero (i.e.,$\tau = 0$, $\omega = 3.6$, $\mu = 0.05$, $\gamma = 0$, $\zeta = 0$, $\beta = 0$), (**a**) the effect of the linear position gain when $\gamma = -2, -0.1, 2$, (**b**) the system time response conferring to (**a**) when $\sigma = -0.5$ (i.e., $\Omega = \omega - 0.5$).

Equations (34) and (35) describe the modulation amplitude a and the modified phase φ for the primary resonance case. In light of the analytical solutions of these equations, we can obtain steady-state solutions in this stage. The analytical solution of Equation (28) with the addition of Equation (31) for selected values $\omega = 3.6$, $\mu = 0.05$, $\gamma = 1.5$, $\alpha = 0$, $\zeta = 0$, $\beta = 0$, $\tau = 0$, $f = 0.5$, and $\sigma = 0$ of the system parameters is plotted in Figure 4a, while the drawn curve in Figure 4b shows the time record of oscillations achieved in Equation (1). It is obvious that the temporal history of the drawn curves in Figure 4b starts at $t = 0$ and then they have a beam of oscillation around the time axis to constitute symmetric vibration around this axis. Therefore, their behaviors have stable procedures.

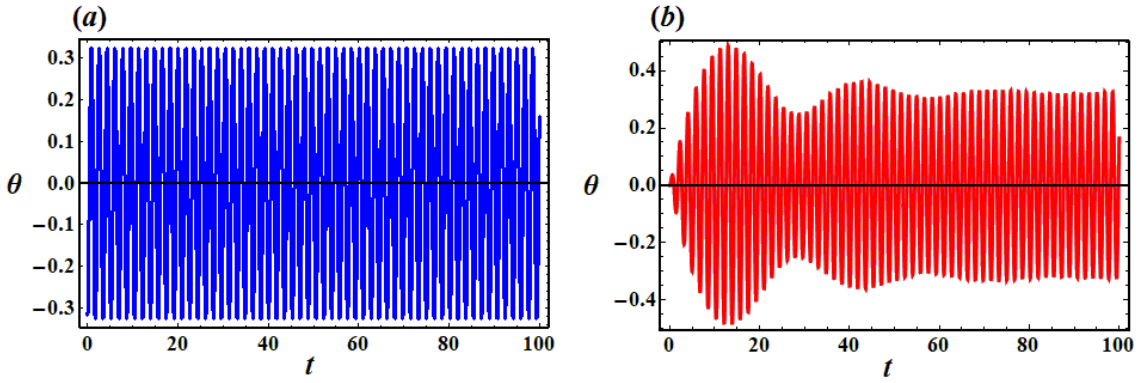

Figure 4. (**a**) Analytic time response when $\omega = 3.6$, $\mu = 0.05$, $\gamma = 1.5$, $\alpha = 0$, $\zeta = 0$, $\beta = 0$, $\tau = 0$, $f = 0.5$, $\sigma = 0$; (**b**) numerical time response at the same value as the analytical solution.

3.2.3. Influence of Linear Position Control with Time-Delay

The outcome of the loop delay on the oscillation control effectiveness of the anticipated linear control is examined here as well as the assistance of the resulting Equations (34) and (35). To examine the presentation of the time-delayed linear position control in controlling the nonlinear vibrations of the structure, the stability graph is achieved by calculating the controller gain Δ against the parameter κ to demonstrate the stable/unstable zones in the $(\Delta - \kappa)$ plane as indicated in Figure 5a. It is obvious in Figure 5a that the unstable zone is replicated uniformly combined with the κ-axis for amounts of Δ. Consequently, it is likely to choose the parameter κ corresponding to Figure 5a for the positive estimates of Δ in a manner that ensures the scheme stability. Figure 5b displays the system FRC when $\gamma = 1$ at three various amounts of the loop delay τ that is chosen in the interior stable/unstable zone corresponding to Figure 5a, i.e., ($\tau = 0.5, 0.8$, and 1.3). It is obvious in Figure 5b that the loop delay can perform a major control in reducing the oscillation amplitude in the situation of $\tau = 0.5$ when $\gamma = 1$, and $\tau = 0.8$ when $\gamma = 1$. It is obvious that the least oscillation stage happens at $\tau = 0.5$, as seen in Figure 6a, while the structure responds with huge oscillation amplitudes at $\tau = 0.8$, as drawn in Figure 6b. Comparing various values of delay in Figure 5b, it is realized that the greatest oscillation decrease level happens at $\tau = 0.5$. Consequently, one can reduce the oscillation of the control utilizing the loop delays as a new-found control parameter. The greatest amount of the loop delay τ that can advance the controller effectiveness would be chosen inside the center of the stable zone. We find this point is in the center of a stable solution zone that is situated concerning two successive unstable areas.

To confirm the accuracy of the stability maps in Figure 5a, a calculation for the structure corresponding to the two values of delay is accomplished by explaining Equation (1), as shown in Figure 6a,b. Therefore, one can observe the structure response as well as uniform vibration amplitude, as in Figure 6a,b. The reason goes back to the points that are designated within the stable zone.

3.2.4. Influence of Linear–Nonlinear Position Control with/without Time-Delay

In what follows, the impact of the two control gains γ and β on the oscillating performances of the system is investigated when the loop delay is (i.e., $\tau = 0, 0.5$). By examining Figure 7a, it is obvious that both the linear position and nonlinear position affect modifying the oscillation by time-delay of the structure. In Figure 7a, we can deduce that the highest efficiency to reduce the amplitude is the linear and nonlinear position controller together with time delay. Figure 7b illustrates the time history corresponding to Figure 7a when $\sigma = 0.0$ at two various amounts of the loop delay $\tau = 0$ and $\tau = 0.5$. The picture shows the great impact of the loop delay on the oscillation amplitudes, where the structure replies with an oscillation amplitude at $\tau = 0$ that is twice in the case of $\tau = 0.5$. Furthermore, the amplitudes of the plotted waves lessened with the increase in τ values, while the

fluctuations numeral remained stationary, which is in high consistency with the analytic solution obtained through Equations (28) and (31).

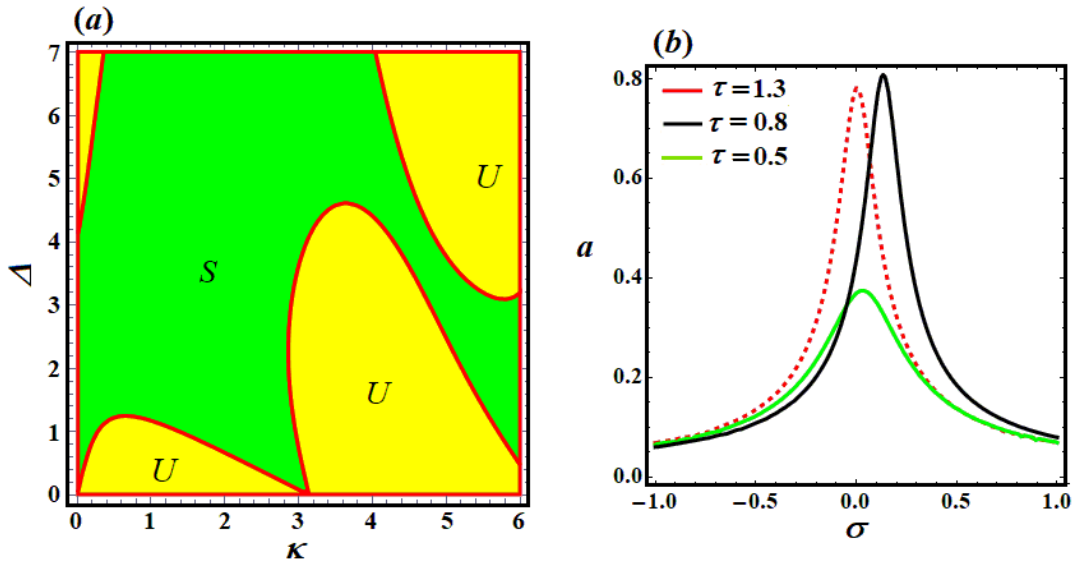

Figure 5. (**a**) The controlled structure stability charts in $(\kappa - \Delta)$ plane, (**b**) The regulated structure FRC corresponding to (**a**) at three distinct amounts of the loop delay.

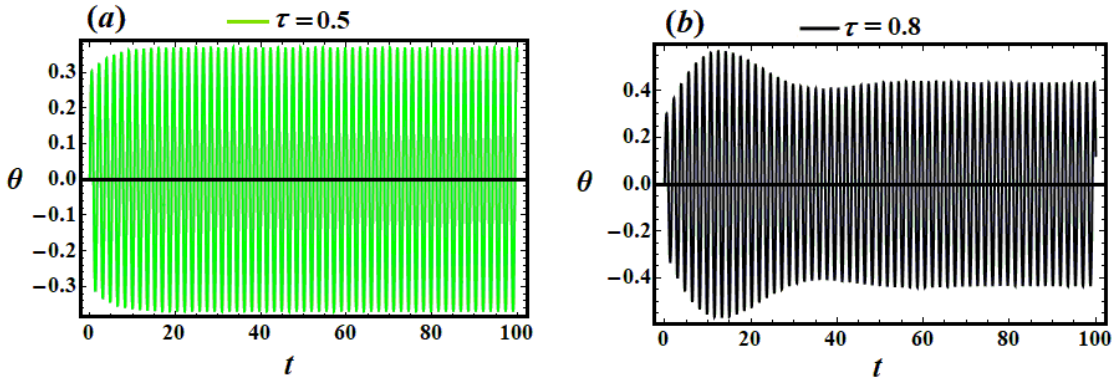

Figure 6. (**a**) The scheme time history when $\tau = 0.5$ (**b**) The system time history when $\tau = 0.8$.

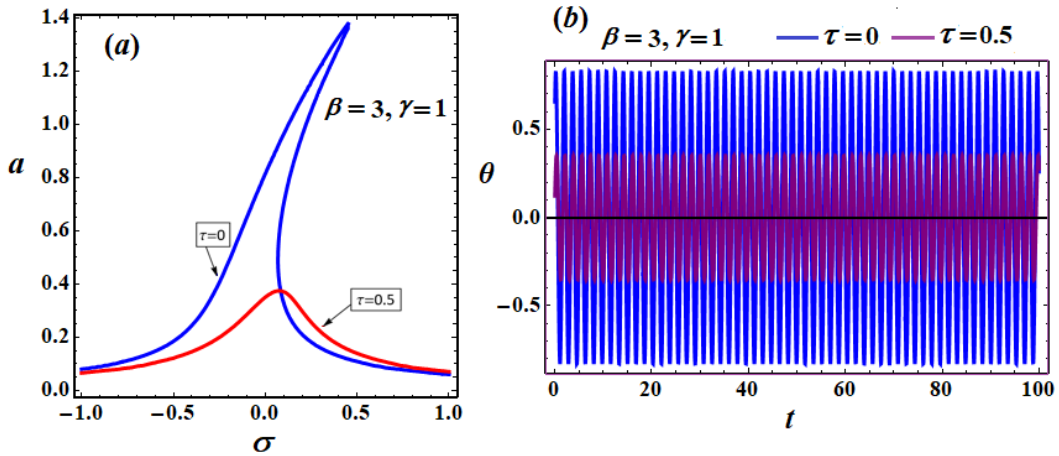

Figure 7. (**a**) The linear and nonlinear position controller structure FRC according to two various amounts of the loop delay, (**b**) the behavior of $\theta(t)$ at $\omega = 3.6$, $\mu = 0.05$, $\gamma = 1$, $\alpha = 0$, $\zeta = 0$, $\beta = 3$, $\tau = 0$, $f = 0.5$, $\sigma = 0$.

3.2.5. Influence of Linear Velocity Control without Time-Delay

Figure 8a demonstrates the impact of lessening the linear speed feedback gain ζ on the FRC, where the decreasing ζ enhances the linear damping factor, which eventually reduces the oscillation amplitudes. The plotted curves have symmetric shapes about the vertical axis $\sigma = 0$, where the amplitude of the produced waves increases with the rise in ζ. The nonlinear temporal oscillation of the beam structure when reducing the speed feedback gain as of $\zeta = -0.2$ to $\zeta = -0.4$ corresponding to Figure 8a is validated in Figure 8b. The graphed curves start from the time zero value, after that the amplitudes of the waves increase with time, and then these waves have a stable manner through the examined time interval. Matching Figure 8a with Figure 8b, one obtains a good correspondence connecting the behaviors of the drawn figures.

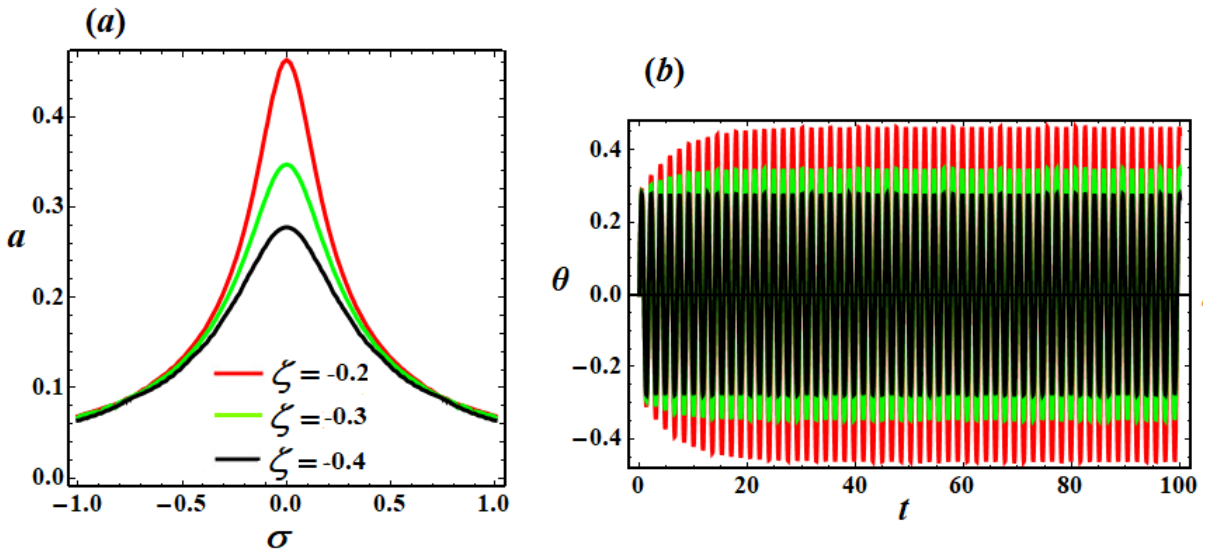

Figure 8. The impact of linear speed response gain of the structure FRC when the loop delay vanishes (i.e., $\tau = 0.0$): (**a**) the effect of the linear velocity gain ζ at $\omega = 3.6$, $\mu = 0.05$, $\gamma = 0$, $\alpha = 0$, $\beta = 0$, and $f = 0.5$, (**b**) the structure time reply when $\zeta = -0.2, -0.3$, and -0.4 (i.e., the linear speed control is stimulated merely).

3.2.6. Influence of Linear–Nonlinear Velocity Control with/without Time Delay

It is possible to avoid the construction of high-level vibration amplitude by adjusting the linear speed with nonlinear speed response control. Figure 9a confirms that the linear velocity with a nonlinear speed response controller is further efficient with time delay in mitigating the system's nonlinear oscillations. By investigating the graph, it is obvious that the lowest vibration stage occurs when $\tau = 0.5$, even though the structure vibrates by large oscillation amplitude. Figure 9b illustrates numerically that each of the linear speed and nonlinear velocity have suppressed the oscillation amplitude when $\varsigma = -0.1$, and $\alpha = 0.5$. By comparing Figure 9a with Figure 9b, one obtains a good understanding of connecting the behaviors of their plotted curves, where the amplitudes increase gradually till a convinced amount of time, and then they will be stationary over the rest of the entire time period.

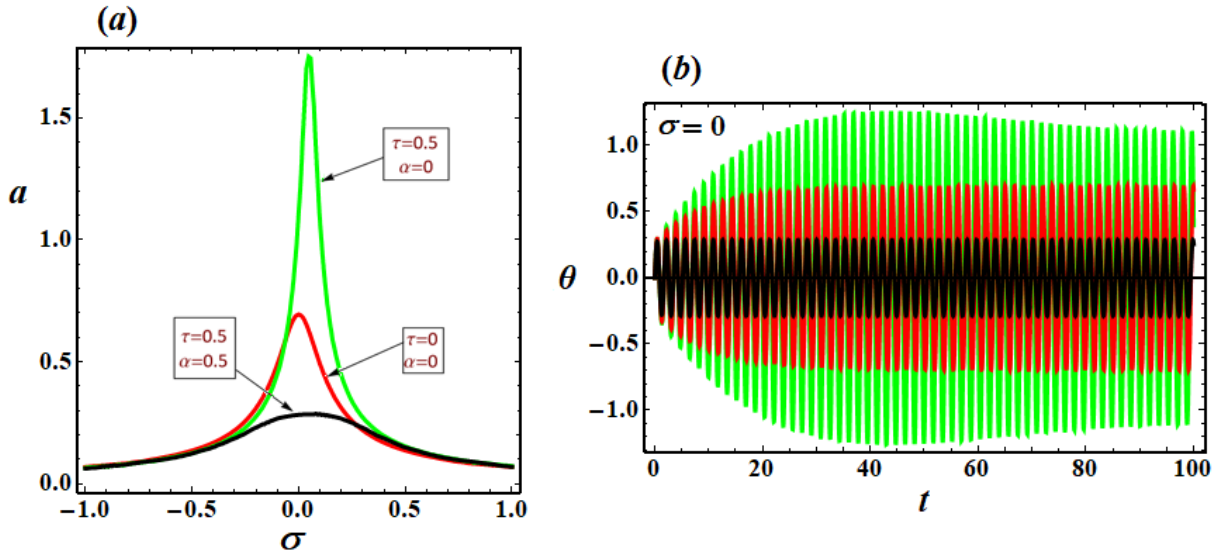

Figure 9. (**a**) The impact of linear velocity with nonlinear velocity response gain of the system FRC once the loop delay is (i.e.,$\tau = 0, 0.5$) at $\omega = 3.6$, $\mu = 0.05$, $\gamma = 0$, $\beta = 0$, and $f = 0.5$, (**b**) the system time response.

4. Conclusions

To mitigate nonlinearity in an excited DO, the current approach introduces a time-delayed position and velocity, serving as an additional method to suppress nonlinear oscillations. While time-delayed systems have been widely studied, the focus of this study is particularly significant. The modified HPM is employed to enhance the accuracy of the estimated solution, providing a more precise approximation. The comparison via the numerical solution using MS validates the accuracy of this analytical technique, allowing for a qualitative evaluation of the results. For diverse values of the physical frequency and time-delay factors, the time histories of the solutions are shown. The findings are described concerning the displayed curves. The multiple-scale technique is used to assess the structured nonlinear prototype. It has looked at the impact of different regulatory thresholds on the organization's vibration effectiveness. The impact of the practical settings on the modulations derived, under these conditions, has been systematically examined. The time-delayed location velocity (linear-nonlinear) response control has been suggested in this study to reduce the system oscillation. The amplitude-phase modulation equations guiding the dynamics of the system at initial resonance have been obtained using the many-scales homotopy technique. The system force and FRC are produced under various parameter settings. The stability diagram and response curves have been used to investigate the effects of the loop delay on the system stability and control performance. The suggested controller's best vibration suppression effectiveness has been presented. The following are some conclusions drawn from the discussion above:

1. As the stimulation frequency is equivalent to the normal frequency of the problem under consideration, the system responds with strong vibration amplitudes.
2. By raising the linear dampening factor at the initial resonance situation, raising the control speed gain can reduce the transverse vibrations.
3. The position velocity linear control presentation is significantly impacted by the inclusion of time delay in the controller loop.
4. The suggested controller vibration suppression effectiveness will be maximized by choosing the loop delays in a way that optimizes the linear/nonlinear dampening factors.
5. As damping controllers, the linear velocity and cubic velocity response controls can reduce system oscillations by changing the system motion characteristics.
6. When a loop delay is proposed, the cubic velocity response control has the maximum effectiveness in controlling the system's nonlinear oscillations.

7. The presence of time delays in the controller loop has a significant impact on how well or poorly the suggested controller works.

As a progress work, similar dynamical systems like the current paper can be analyzed via a novel methodology named the non-perturbative approach. This concept simply converts any nonlinear ODE into a linear one. Therefore, instead of handling the nonlinear equation, one can examine the comparative linear ODE. Furthermore, in view of the novel approach, the coupled system can also be investigated.

Author Contributions: K.A.: Resources, Methodology, Formal analysis, Validation, Visualization and Reviewing. G.M.M.: Conceptualization, Resources, Methodology, Formal analysis, Validation, Writing—Original draft preparation, Visualization and Reviewing. T.S.A.: Investigation, Methodology, Data duration, Conceptualization, Validation, Reviewing and Editing. A.A.G.: Examination, Organization, Data duration, Validation, Corroboration, Rereading and Editing. All authors have read and agreed to the published version of the manuscript.

Funding: This research was funded by Researchers Supporting Project number (RSPD2024R588), King Saud University, Riyadh, Saudi Arabia.

Data Availability Statement: All data generated or analyzed during this study are included in this published article.

Acknowledgments: The authors extend their appreciation to Researchers Supporting Project number (RSPD2024R588), King Saud University, Riyadh, Saudi Arabia.

Conflicts of Interest: The authors have not revealed any conflicting interests.

List of Symbols

θ	Displacement.
$\cdot$	Time derivative.
ω	Natural frequency.
μ	Linear damping coefficient.
α	Pure cubic damping coefficient.
β	Cubic nonlinear Duffing coefficient, where $\beta > 0$, $\beta < 0$ refer to hardening and softening spring, correspondingly.
f	Excited force.
Ω	Force's frequency.
γ	Position time-delay coefficient.
ζ	Velocity time-delay coefficient.
τ	Time-decay control.
δ, ρ	Small artificial factors.

References

1. Siewe, M.S.; Tchawoua, C.; Woafo, P. Melnikov chaos in a periodically driven Rayleigh-Duffing oscillator. *Mech. Res. Commun.* **2010**, *37*, 363–368. [CrossRef]
2. Siewe, M.S.; Cao, H.J.; Sanjuán, M.A.F. Effect of nonlinear dissipation on the basin boundaries of a driven two-well Rayleigh-Duffing oscillator. *Chaos Solitons Fractals* **2009**, *39*, 1092–1099. [CrossRef]
3. Felix, J.L.P.; Balthazar, J.M.; Brasil, R.M.L.R.F. Comments on nonlinear dynamics of a non-ideal Duffing–Rayleigh oscillator: Numerical and analytical approaches. *J. Sound Vib.* **2009**, *319*, 1136–1149. [CrossRef]
4. Yue, X.; Xu, W.; Zhang, Y. Global bifurcation analysis of Rayleigh-Duffing oscillator through the composite cell coordinate system method. *Nonlinear Dyn.* **2012**, *69*, 437–457. [CrossRef]
5. Wang, Z.; Chen, H.; Tang, Y. The focus case of a nonsmooth Rayleigh–Duffing oscillator. *Nonlinear Dyn.* **2022**, *107*, 269–311. [CrossRef]
6. Akbari, M.R.; Ganji, D.D.; Majidian, A.; Ahmadi, A.R. Solving nonlinear differential equations of Vanderpol, Rayleigh and Duffing by AGM. *Front. Mech. Eng.* **2014**, *9*, 177–190. [CrossRef]
7. Giné, J.; Valls, C. On the dynamics of the Rayleigh–Duffing oscillator. *Nonlinear Anal. Real World Appl.* **2019**, *45*, 309–319. [CrossRef]
8. Mondal, A.; Islam, N. Study on dynamical system with time-delay. *J. Appl. Nonlinear Dyn.* **2016**, *5*, 441–456. [CrossRef]

9. Koshkoueia, A.J.; Farahib, M.H.; Burnham, K.J. An almost optimal control design method for nonlinear time-delay systems. *Int. J. Control* **2012**, *85*, 147–158. [CrossRef]
10. Farahi, M.H.; Barati, S. Fuzzy time-delay dynamical systems. *J. Math. Comput. Sci.* **2011**, *2*, 44–53. [CrossRef]
11. Haddada, W.M.; Chellaboina, V.S. Stability theory for nonnegative and compartmental dynamical systems with time delay. *Syst. Control. Lett.* **2004**, *51*, 355–361. [CrossRef]
12. Kamath, A.G. The Stability Analysis of Linear Dynamical Systems with Time-Delays. Ph.D. Dissertation, The University of Tennessee, Knoxville, TN, SA, 2006.
13. Leylaz, G.; Wang, S.; Sun, J.-Q. Identification of nonlinear dynamical systems with time delay. *Int. J. Dyn. Control.* **2022**, *10*, 13–24. [CrossRef]
14. Yang, T.; Cao, Q. Noise-induced phenomena in a versatile class of prototype dynamical system with time delay. *Nonlinear Dyn.* **2018**, *92*, 511–529. [CrossRef]
15. He, J.H. Homotopy perturbation technique. *Comput. Methods Appl. Mech. Eng.* **1999**, *178*, 257–262. [CrossRef]
16. He, J.H. A coupling method of a homotopy technique and a perturbation technique for non-linear problems. *Int. J. Non-Linear Mech.* **2000**, *35*, 37–43. [CrossRef]
17. Ayati, Z.; Biazar, J. On the convergence of Homotopy perturbation method. *J. Egypt. Math. Soc.* **2015**, *23*, 424–428. [CrossRef]
18. Moatimid, G.M. Stability Analysis of a parametric Duffing oscillator. *J. Eng. Mech.* **2020**, *146*, 05020001. [CrossRef]
19. Moatimid, G.M.; Amer, T.S. Analytical approximate solutions of a magnetic spherical pendulum: Stability analysis. *J. Vib. Eng. Technol.* **2023**, *11*, 2155–2165. [CrossRef]
20. Moatimid, G.M.; Amer, T.S.; Zekry, M.H. Analytical and numerical study of a vibrating magnetic inverted pendulum. *Arch. Appl. Mech.* **2023**, *93*, 2533–2547. [CrossRef]
21. El-Dib, Y.O.; Moatimid, G.M. Stability configuration of a rocking rigid rod over a circular surface using the homotopy perturbation method and Laplace transform. *Arab. J. Sci. Eng.* **2019**, *44*, 6581–6591. [CrossRef]
22. Ghanem, S.; Amer, T.S.; Amer, W.S.; Elnaggar, S.; Galal, A.A. Analyzing the motion of a forced oscillating system on the verge of resonance. *J. Low Freq. Noise Vib. Act. Control.* **2023**, *42*, 563–578. [CrossRef]
23. He, J.-H.; Amer, T.S.; Abolila, A.F.; Galal, A.A. Stability of three degrees-of-freedom auto-parametric system. *Alex. Eng. J.* **2022**, *61*, 8393–8415. [CrossRef]
24. Nayfeh, A.H. *Perturbations Methods*; Wiley-VCH Verlag GmbH and Co. KGaA: Weinheim, Germany, 2004.
25. Starosta, R.; Kamińska, G.S.; Awrejcewicz, J. Asymptotic analysis of kinematically excited dynamical systems near resonances. *Nonlinear Dyn.* **2012**, *68*, 459–469. [CrossRef]

Disclaimer/Publisher's Note: The statements, opinions and data contained in all publications are solely those of the individual author(s) and contributor(s) and not of MDPI and/or the editor(s). MDPI and/or the editor(s) disclaim responsibility for any injury to people or property resulting from any ideas, methods, instructions or products referred to in the content.